A Combined Experimental and Numerical Investigation of Linear Driving Force Kinetics in Small Activated Carbon Beds

Samuel G. A. Wood[a], Nilanjan Chakraborty[a], Martin W. Smith[b], Mark J. Summers[b]*

[a]School of Engineering, Newcastle University, Newcastle upon Tyne, NE1 7RU, UK

[b]Defence Science and Technology Laboratory, Porton Down, Salisbury, SP4 0JQ, UK

*s.wood8@ncl.ac.uk

Abstract

A numerical model has been developed with the intention of better understanding the relationship between flow characteristics and adsorption behaviour in small activated carbon beds. The model uses the Dubinin-Radushkevich adsorption isotherm with Linear Driving Force kinetics and has been validated against experimental data for the breakthrough of cyclohexane. Simulations have been carried out varying the inlet flow rate and the adsorption kinetic constant. The adsorption behaviour has been analysed by assessing the furthest point into the bed that a threshold concentration of contaminant could be seen in the vapour phase. It was seen in all cases that the adsorption was a two stage process, with a rapid initial penetration into a certain bed depth, followed by a relatively slow gradual progression of the front through the bed over time. The initial

distance penetrated into the bed has been seen to be inversely proportional to the kinetic constant, the same trend as predicted from a plug flow mass balance analysis. The rate of steady front advancement after this showed a slight tendency to increase with decreasing adsorption kinetics, compared to the expected plug flow speed.

Keywords: Reynolds-Averaged Navier-Stokes, activated carbon, adsorption, Linear Driving Force kinetics

Introduction

Activated carbon is extensively used as an adsorbent due to its low cost and excellent adsorption properties. In many applications, such as in respiratory protection or the treating of industrial outflows, a bed of activated carbon is used to clean a gas stream to wholly prevent the penetration of a contaminant downstream. In this situation, contaminant will advance from the inlet of the carbon bed until it finally reaches the outlet (usually termed "breakthrough"), at which time the bed is deemed to be exhausted and needs replacement.

There are a number of experimental studies which investigate the breakthrough behaviour of a range of common contaminants on activated carbon beds[1-3]. Existing breakthrough models are largely used under the assumption that the contaminant flow through the bed will follow plug flow behaviour, with no velocity variations in the radial direction. In reality, the flow field will be affected by the bed geometry. There is therefore a need for a better understanding between the relationship between the flow field and the breakthrough characteristics of a bed.

Activated carbons feature complex disordered surfaces, which provide a strong adsorption potential. The physical basis of adsorption of gases is an attraction due to a potential, which is dependent on the spatial position of the gas molecules relative to the adsorbent surface. The vapour, once adsorbed, has liquid-like properties and occupies volume on the adsorbent material, which in turn affects the adsorption-force field[4]. This reduces the driving force for adsorption as the adsorbent becomes more loaded, until an equilibrium uptake is reached, which depends on the local vapour concentration of the adsorbate molecule[5-6]. There are a large number of models[7] describing physical adsorption of vapours onto microporous solids.

The Dubinin-Radushkevich equation is a semi-empirical model which has been extensively used to model adsorption of organic vapours onto activated carbon[7]. The equilibrium uptake W_e (g vapour/g carbon) is expressed as follows[8-9]:

$$W_e = \rho_L W_0 \exp[-\left(\left(\frac{RT}{\beta E_o}\right)\ln\left(\frac{p_{sat}}{p}\right)^2\right) \quad (1)$$

where W_0 is the volume of micropores per unit mass of activated carbon, ρ_L is the density of the adsorbed material in the liquid phase, βE_0 is the adsorption energy, p_{sat} is the saturation vapour pressure of the adsorbate and p the local adsorbate partial pressure.

While the Dubinin-Radushkevich equation describes the thermodynamic driving force for adsorption, adsorption rate will also be kinetically limited. Previous studies on activated carbon have revealed that for a very wide variety of volatile organic compounds the adsorption rate is limited by intra-particle diffusion through the carbon. In these cases, the Linear Driving Force (LDF) kinetic model is applicable over the entire relevant area of the adsorption isotherm[10-11]. Under the LDF model, the rate of change in uptake adsorbed is:

$$\frac{dW}{dt} = K_M(W_e - W) \quad (2)$$

where K_M is the effective mass transfer kinetic constant, which is highly dependent on the adsorbate material for volatile organic compounds adsorbing to activated carbon.

It is clearly desirable to maximize the working lifetime of activated carbon beds. Optimum usage of an activated carbon bed would occur when all of the adsorbed contaminant is at total equilibrium with the inlet concentration throughout the whole bed, before any breakthrough into the outlet stream is seen. This situation is unrealistic however, as it depends on instant adsorption kinetics and perfect plug flow throughout the bed. This must therefore be taken into account by any models which seek to predict carbon bed breakthrough times. A commonly used model which estimates breakthrough time t_b for a bed of length L with a mean inlet velocity V_L, with inlet concentration

C_{in} and target breakthrough concentration C_{out} is the Wheeler-Jonas equation, which is derived from a mass balance over the carbon bed[12-14].

$$t_b = \frac{\rho_B W_e}{C_{in} V_L}\left[L - \frac{V_L}{k_{WJ}} \ln\left(\frac{C_{in}}{C_{out}}\right)\right] \quad (3)$$

The kinetic constant k_{WJ} for the Wheeler-Jonas equation can be estimated using a number of methods, such as that proposed by Lodewyckx *et al*[8, 15]:

$$k_{WJ} = 800\ \beta^{0.33} V_L^{0.75} d_p^{-1.5} \sqrt{\frac{W_e}{M_W}} \quad (4)$$

Here, β is the affinity coefficient of a given adsorbate (the same as that seen in Eq. 1) and is found experimentally. This correlation has been extensively used and shown to give good results for the adsorption of organic vapors onto activated carbon beds[16-18].

In reality, the flow through the bed will be affected by the bed geometry. In large beds of porous material, the axial radial velocity profile is expected to be near plug flow, with a thin boundary layer adjacent to the wall[19]. In this case, the plug flow assumption used in the Wheeler-Jonas model will be approximately valid. However, in the case of small beds (or faster axial velocities), it is expected that a greater proportion of the flow will be within the boundary layer, and there will hence be a greater deviation from plug flow. Under plug flow conditions, the axial concentration profile associated with adsorption kinetics is well understood[12]. As the velocity profile deviates from plug flow, there will be coupling between the adsorption kinetics and the flow field, as adsorption reduces the fluid volume flow rate and hence its velocity. Likewise, the fluid velocity will affect the local concentration and residence time and hence the degree of adsorption. It is therefore useful to gain better understanding of flow characteristics in adsorbent beds. This is achieved by carrying out a detailed Computational Fluid Dynamics (CFD) analysis in this study.

CFD has previously been used to predict flow profiles in activated carbon beds, particularly in the case of CBRN filter canisters[20-21]. Additionally, some adsorption modelling using CFD in a similar application has also been carried out[22]. There is considerable potential to improve CBRN canister design in order to improve both the service life and the pressure drop across the filter. At present, a minimum service life of 5 minutes when exposed to a standardized range of test contaminants at an inlet flowrate of 100 l min^{-1}, although many filters will aim to greatly exceed this. This standard must be met in addition to maintaining a pressure drop of less than 784 Pa. In general, thicker filters will increase the service life while also increasing the pressure drop. Improved understanding of flow and adsorption behavior within the filter would allow designs which make better use of the existing filter material without increasing pressure drop[23].

The purpose of this study is to understand the coupled relationship between the adsorption kinetics and the flow profile throughout the bed and relate this to the breakthrough time.

Understanding of the flow profile is achieved by means of unsteady Reynolds Averaged Navier-Stokes simulations, which incorporate the previously discussed adsorption process. This relationship can then be used to identify how a carbon bed will perform for a range of target adsorptives without the need for detailed adsorption modelling, with the objective of optimizing future adsorbent bed designs. This would also more easily allow for predicting the behaviors of novel adsorbent materials, such as ordered mesoporous carbons (OMCs) which show improved adsorption kinetics over existing activated carbons[24].

In this study, an experimentally determined isotherm for cyclohexane on activated carbon has been used as the basis for CFD simulations to predict adsorption behavior over a variety of inlet flow rates through a cylindrical packed bed of granular activated carbon. These simulations were

then repeated, but with modified values of K_M, the LDF kinetic constant, to see how the adsorption kinetics affected the flow field and adsorption performance.

The simulations were validated by conducting experiments to find the breakthrough time of various depths of carbon bed at different flow rates.

Experimental Method and Results

Isotherm data has been measured using a DVS Advantage from Surface Measurement Systems. A small mass of dry granular activated carbon (approximately 25mg, supplied by Emcel Filters Ltd) was exposed to a regulated continuous stream of dry air at 298K. A stream of air contaminated by a known concentration of cyclohexane was then introduced and the change in mass of the activated carbon relative to an inert reference sample was recorded as cyclohexane was adsorbed. When the mass of the carbon remained unchanged for ten minutes the uptake was recorded. The inlet cyclohexane concentration was then increased until the full range of relative pressure (up to p/p_{sat} = 0.95) had been covered. Isotherm measurement takes place under automatic control from the instrument software.

This isotherm data (in the p/p_{sat} range of 0.0 – 0.2) was then fitted to the Dubinin-Radushkevich equation (Eq. 1) to identify best-fit values of W_0 and βE_0, the adsorption energy. The experimental isotherm results and the fitted Dubinin-Radushkevich equation can be seen in Fig. 1. The fitted Dubinin-Radushkevich equation clearly gives a close representation of the experimental data, and is therefore used in the numerical component of this study.

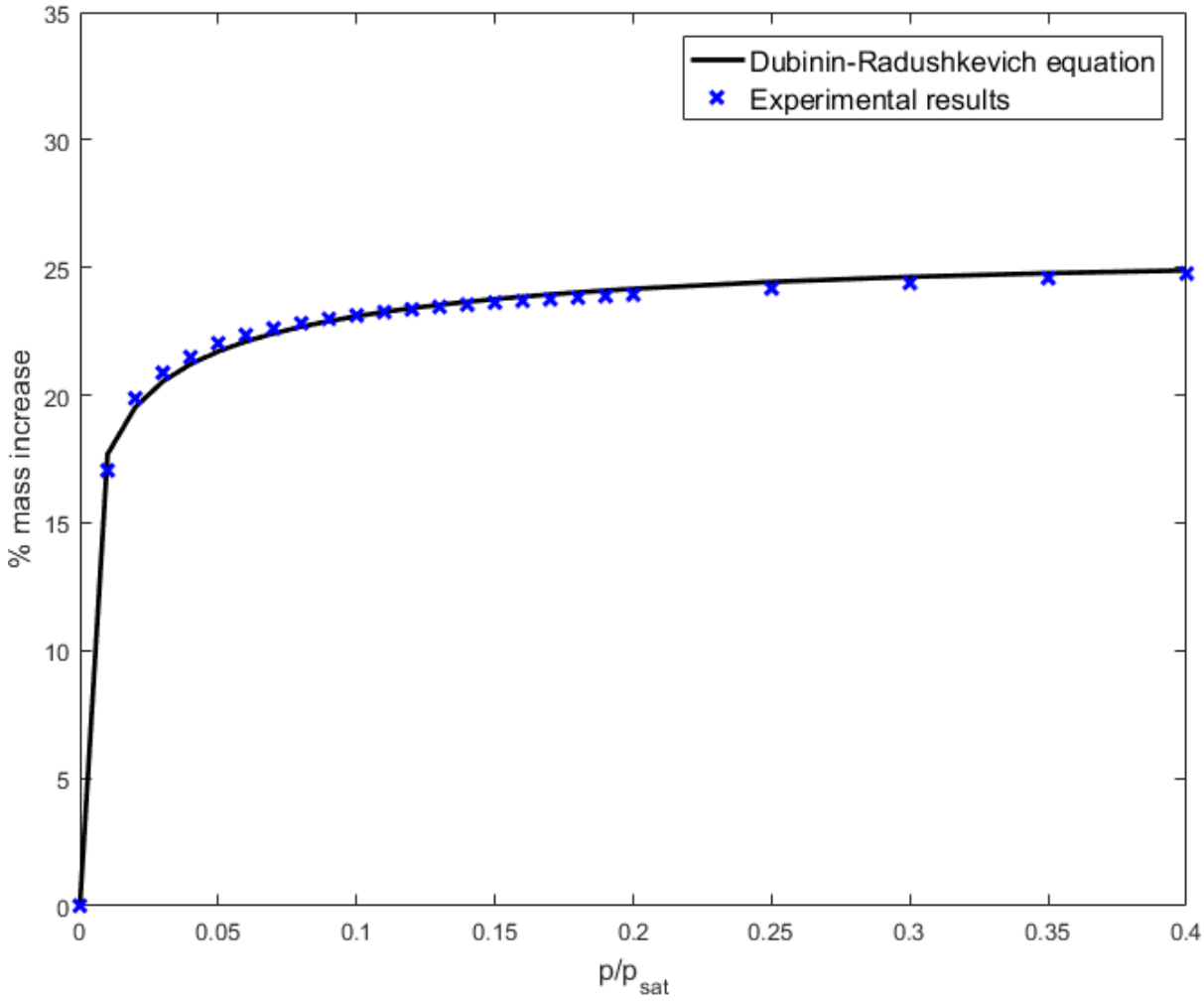

Figure 1: The adsorption isotherm for cyclohexane on activated carbon at 295K and the mass uptake predicted using the Dubinin-Radushkevich equation fitted to this experimental data.

Cylindrical carbon beds with a diameter of 86.5 mm and depths of 15 mm were used to evaluate the breakthrough time of cyclohexane. The beds were packed using the snowstorm filling technique[25] with activated carbon of a mean particle size of 1 mm and a nominal density of 550 kg m^{-3}. The particles exhibited a high degree of heterogeneity with respect to size and shape.

A continuous stream of dry air at flow rates of 15, 30 and 50 l min^{-1} (corresponding to inlet velocities of 0.0425, 0.0851 and 0.142 m/s respectively) was drawn through fixed beds of clean activated carbon for a duration sufficient to measure a steady baseline reading at a sampling mass

spectrometer at the outlet. An influent concentration of 2000 ppm was then introduced to the air stream. The concentration of cyclohexane in the outlet was measured by mass spectrometry (monitoring for the mass-to-charge ratio m/z=84, the molecular ion for cyclohexane) at one second intervals until a clear breakthrough was observed. The results of this are shown in Fig. 2.

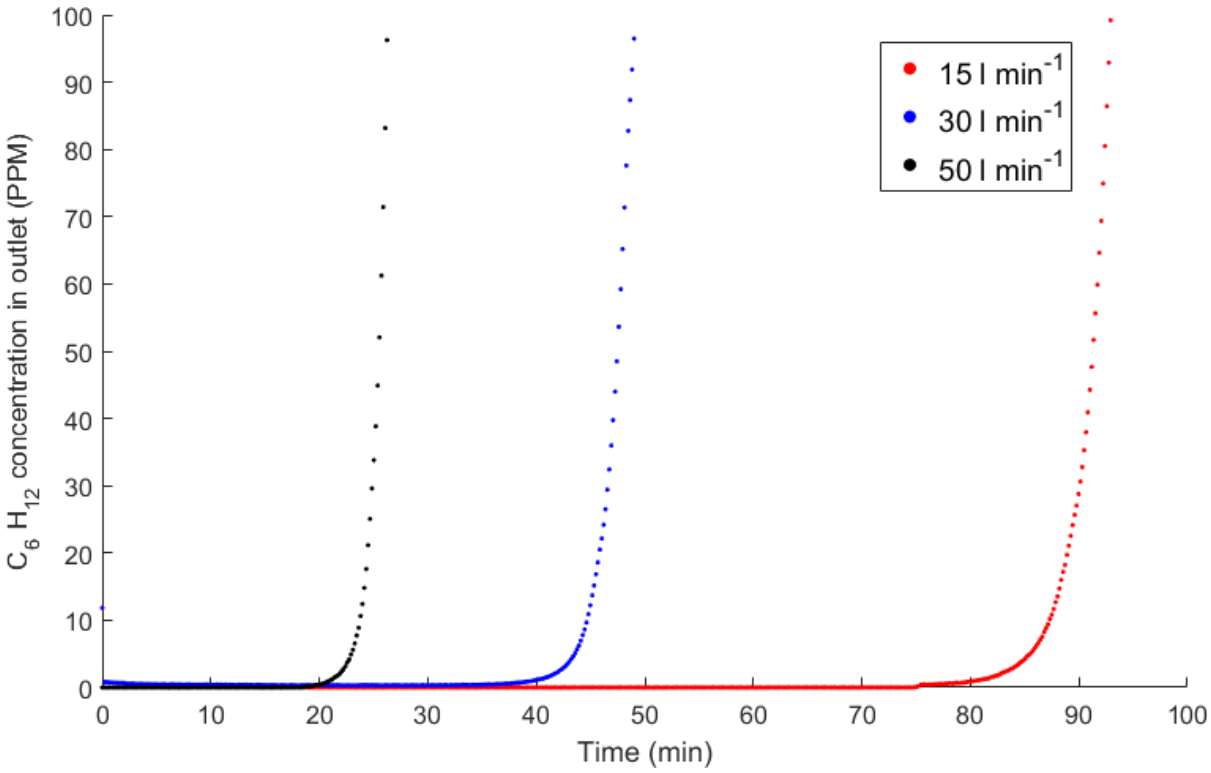

Figure 2: Outlet stream concentration of cyclohexane for a 15 mm activated carbon bed exposed to three different inlet flow rates with a concentration of 2000 ppm.

Numerical Implementation

Simulations have been carried out using Ansys Fluent[26] to solve the modelled unsteady Reynolds averaged equations for the conservation of mass, momentum, energy and species throughout the domain using the finite volume method. All the advective and diffusive terms have been discretized using the second order upwind scheme and second order central differencing schemes, respectively. The link between pressure and velocity has been accounted for by the use of the

SIMPLE algorithm[27]. The convergence criteria have been given by a scaled residual of 10^{-6} for the energy equation and 10^{-4} for all other equations.

The Reynolds-averaged Navier-Stokes (RANS) equations have been used for the simulations. This requires each variable to be separated into a mean and fluctuating component. The Reynolds-averaged mass conservation equation for incompressible fluids can then be written as:

$$\frac{\partial \rho}{\partial t} + \frac{\partial \rho \overline{u_i}}{\partial \mathrm{x_i}} = \bar{S}_{mi} \tag{5}$$

where u_i is the velocity in the ith direction and $\bar{S}_{mi}$ is a source term which relates to the adsorption process:

$$\bar{S}_{mi} = K_M \rho_s (W - W_e) \tag{6}$$

Here, W_e is the equilibrium uptake as given by Eq. 1. This equation has been selected due to its widespread use with volatile organic compounds and its good match to the experimental data[7]. The cumulative uptake $W = \sum \frac{dW}{dt} \delta t$ is stored for each cell and given by Eq. 2.

The Reynolds-averaged momentum conservation equation is:

$$\frac{\partial}{\partial \mathrm{t}} (\rho \overline{u}_i) + \frac{\partial}{\partial x_j} \left(\rho \overline{u}_i \overline{u}_j \right) = \frac{\partial}{\partial x_j} \left[\mu_l \frac{\partial \overline{u}_i}{\partial x_j} \right] - \frac{\partial \bar{p}}{\partial x_i} - \frac{\partial}{\partial x_j} \left(\overline{\rho u_i' u_j'} \right) + \bar{S}_{ui} \tag{7}$$

where ρ and μ_l are the density and dynamic viscosity respectively. The equation remains unclosed due to the Reynold's stress term $\left(-\overline{\rho u_i' u_j'} \right)$, which must be modelled by the use of an appropriate turbulence model. The source term $\bar{S}_{ui}$ originates from the viscous and inertial resistance of the porous medium:

$$\bar{S}_{ui} = a_1 V_{i,s} + a_2 V_{i,s}^2 \tag{8}$$

where a_1 and a_2 are the viscous and inertial resistances specific to the porous medium and $V_{i,s}$ is the superficial fluid velocity in the i[th] direction.

The Reynolds averaged species conservation for species a with mass fraction α is given by:

$$\frac{\partial}{\partial t}(\rho\bar{\alpha}) + \frac{\partial}{\partial x_i}(\rho\bar{u}_i\bar{\alpha}) = -\frac{\partial}{\partial x_i}\overline{J_{\alpha,\imath}} - \frac{\partial}{\partial x_i}\left(\rho\overline{u_\imath'\alpha'}\right) + \bar{S}_{\alpha,i} \tag{9}$$

$$\overline{J_{a,\imath}} + \rho\overline{u_\imath'\alpha'} = -\left(\rho D_{a,m} + \frac{\mu_t}{Sc_t}\right)\frac{\partial\bar{\alpha}}{\partial x_i} \tag{10}$$

where $D_{a,m}$ is the mass diffusion coefficient and $Sc_t = 0.9$ is the turbulent Schmidt number ($\mu_t/\rho D_t$). As only one species is adsorbed $\bar{S}_{\alpha,i} = \bar{S}_{m,i}$ as given by Eq. 6.

The transport of energy for turbulent incompressible flows takes the following form:

$$\frac{\partial(\rho\bar{E})}{\partial t} + \frac{\partial}{\partial x_i}(\rho\bar{u}_\imath\bar{E}) = \frac{\partial}{\partial x_i}\left(\underbrace{k_{eff}\frac{\partial\bar{T}}{\partial x_i}}_{conduction} - \underbrace{\sum_a \bar{h}_a\overline{J_{a,\imath}}}_{species\ diffusion}\right) + \underbrace{\bar{S}_{ei}}_{heat\ of\ adsorption} \tag{11}$$

where E is the specific internal energy and $k_{eff} = k + c_p\mu_t/Pr_t$ is the effective thermal conductivity where $Pr_t = 0.9$ is the turbulent Prandtl number.

The source term $\bar{S}_{ei} = -\beta E_0\bar{S}_{mi}/M_w$ depends on the experimentally measured βE_0 which is given in Table 2.

The Reynolds stress term $-\left(\overline{\rho u_\imath' u_j'}\right)$ seen in Eq. 7 is modelled by a gradient hypothesis:

$$-\left(\overline{\rho u_\imath' u_j'}\right) = \mu_t\left(\frac{\partial\bar{u}_i}{\partial x_j} + \frac{\partial\bar{u}_j}{\partial x_i}\right) - \delta_{ij}\frac{2\rho k}{3} \tag{12}$$

where the eddy viscosity μ_t is expressed by means of turbulent intensity $k = \overline{u_\imath' u_j'}/2$ and its dissipation rate $\epsilon = \overline{\nu(\partial u_\imath'/\partial x_j)(\partial u_\imath'/\partial x_j)}$ in the following manner in the context of $k-\epsilon$ modelling:

$$\mu_t = C_\mu\rho k^2/\epsilon \text{ where } C_\mu = 0.09 \tag{13}$$

However, k and ϵ are unclosed terms and they are evaluated by solving their modelled transport equations, which are given by:

$$\frac{\partial}{\partial \mathrm{t}}(\rho k) + \frac{\partial}{\partial x_j}\left(\rho\bar{u}_j k\right) = \frac{\partial}{\partial x_j}\left[\left(\mu_l + \frac{\mu_t}{\sigma_k}\right)\frac{\partial k}{\partial x_j}\right] + \underbrace{\mu_t\left(\frac{\partial\bar{u}_i}{\partial x_j} + \frac{\partial\bar{u}_{ij}}{\partial x_i}\right)\frac{\partial\bar{u}_i}{\partial x_j}}_{\substack{Turbulent\ kinetic \\ energy\ generation}} - \underbrace{\rho\epsilon}_{\substack{turbulent \\ dissipation}} \tag{14}$$

$$\frac{\partial}{\partial \mathrm{t}}(\rho\epsilon) + \frac{\partial}{\partial x_j}\left(\rho\bar{u}_j\epsilon\right) = \frac{\partial}{\partial x_j}\left[\left(\mu_l + \frac{\mu_t}{\sigma_\epsilon}\right)\frac{\partial\epsilon}{\partial x_j}\right] + \frac{\epsilon}{k}\left[C_{\epsilon 1}\mu_t\left(\frac{\partial\bar{u}_i}{\partial x_j} + \frac{\partial\bar{u}_{ij}}{\partial x_i}\right)\frac{\partial\bar{u}_i}{\partial x_j}\right] - \frac{\rho\,\epsilon^2}{k}C_{\epsilon 2} \tag{15}$$

where $\sigma_k = 1.1$; $\sigma_\epsilon = 1.3$; $C_{\epsilon 1} = 1.44$ and $C_{\epsilon 2} = 1.92$ are constants of the model. The near wall behaviors of k and ϵ are modelled by means of a blended wall approach which has previously been used in the modelling of carbon beds[28], in which the domain is subdivided into a near-wall viscosity affected region and a fully turbulent region according to the local turbulent Reynolds number, Re_y:

$$Re_y = \frac{\rho y \sqrt{k}}{\mu_l} \tag{16}$$

In the near wall region ($Re_y < 200$) a one-equation model is employed, in which the full transport of ϵ is no longer solved but is instead algebraically modelled as:

$$\epsilon = k^{\frac{3}{2}} / l_\epsilon \tag{17}$$

where $l_\epsilon = y C_l^* \left(1 - e^{\frac{-Re_y}{2C_l^*}}\right)$, $C_l^* = \kappa C_\mu^{-\frac{3}{4}}$ and $\kappa = 0.4$. The turbulent viscosity in this region is then calculated as:

$$\mu_{t,nearwall} = \rho C_\mu l_\mu \sqrt{k} \qquad \text{where } l_\mu = y\, C_l^* \left(1 - e^{-\frac{Re_y}{A_\mu}}\right) \text{ and } A_\mu = 70 \tag{18}$$

The turbulent viscosity between the near-wall and fully turbulent regions is blended as follows:

$$\mu_{t,blend} = \lambda_\epsilon \mu_t + (1 - \lambda_\epsilon)\mu_{t,nearwall} \tag{19}$$

$$\lambda_\epsilon = \frac{1}{2}\left[1 + \tanh\left(\frac{Re_y - 200}{A}\right)\right] \tag{20}$$

Here, A is a constant chosen such that λ_ϵ ranges from zero at the wall to one far from the wall.

The local species concentration is subject to effects of fluctuations in the flow field due to turbulence[29]. However, for larger kinetic constants, the adsorption rate would be governed by both the reaction kinetics and the effect of turbulent mixing. For all cases considered here the kinetic constant is far below the threshold required for turbulent mixing to become significant, so the mean values of mass fraction are used to describe the source term for adsorption seen in Eq. 6 without accounting for turbulent fluctuations[30].

The numerical model used here has been used previously used to give good predictions of pressure drop across an activated carbon bed[31].

Mesh independence

Mesh independence has been ensured by assessing the initial depth of penetration into the bed and the speed of the advancing contaminated front for three representative cases. The results are shown in Table 1. The coarser of the two meshes was selected for use in the main study as the results did not change significantly with grid refinement.

Table 1: Results of the mesh independence and validation studies study for the selected cases.

Mesh	**No. of cells in axial direction within carbon bed**	**No. of cells in radial direction within carbon bed**	**No. of cells in axial direction within open pipe**	**No. of cells in radial direction within open pipe**	**Expansion ratio**	**Total number of cells**
A	163	98	142	98	1.1	29890
B	214	115	150	115	1.1	41860

Inlet Flowrate (l min^{-1})	**Inlet velocity (m/s)**	**K_M (s^{-1})**	**Mesh**	**Initial contaminated front length (mm)**	**Contaminated front speed (m/s)**
50	0.142	0.01	A	12.08	1.13×10^{-5}
			B	12.10	1.13×10^{-5}
1000	2.836	0.004	A	57.55	2.11×10^{-4}
			B	57.40	2.11×10^{-4}
1000	2.836	0.01	A	23.30	2.04×10^{-4}
			B	23.34	2.04×10^{-4}

Flowrate (l min^{-1})	**Inlet velocity (m/s)**	**Experimental breakthrough time (s)**	**CFD breakthrough time (s)**
15	0.0425	5208	5010
30	0.0851	2688	2631
50	0.1418	1407	1440

Operating and Boundary Conditions

All simulations have been conducted on an 86.5 mm diameter cylinder as used for the experimental results. For the simulations, a 15 mm packed bed of carbon with 50 mm clear cylinder at the inlet and outlet has been considered to allow the flow to develop fully. All simulations exploited the axisymmetric nature of the geometry to reduce the computational cost.

All cases considered an average bead diameter of 1 mm, as used in the experiments. The carbon bed was treated as a uniform porous medium with a fixed bulk porosity throughout the domain to depict the heterogeneous nature of the carbon used within the experimental study. The viscous and inertial losses which provide the source term for Eq. 8[20]:

$$\bar{S}_{ui} = (-\Delta\bar{p}/L)_{\mathrm{i}} = 2.39\mathrm{x}10^{9}\, V_{s,i} + 3.21\mathrm{x}10^{4}\, V_{s,i}^{2} \qquad (21)$$

where the first term describes the viscous loss and the second term the inertial loss.

Cyclohexane was chosen as the test contaminant, as it is commonly used as a representative agent for a variety of volatile organic compounds in the testing of respirator canisters[23], a common application of shallow activated carbon beds. The inlet flow rate was initially chosen to be 50 l min^{-1} (corresponding to an inlet velocity of 0.142 m/s) as it has been used previously as representative of a human breathing rate[32]. Inlet flow rates up to 1000 l min^{-1} (inlet velocity of 2.836 m/s) were also studied, as it was expected that a greater deviation from the plug flow assumption at higher flow rates. The relevant properties of cyclohexane at 295 K are given in Table 2.

Table 2: Physical properties used for this study

Cyclohexane Molecular Weight (kmol/kg)	84.17
Cyclohexane Diffusion Coefficient in air[33] (m^2/s)	$7.84x10^{-6}$
Heat of adsorption (kJ/kmol)*	18945.5
Micropore volume (cm^3 micropore/g carbon)*	0.324
Effective mass transfer coefficient (s^{-1})[8, 15]	0.004
Bulk porosity (-)	0.365
Bulk Density (kg/m^3)	550
Mean particle diameter (m)	0.001

*taken from the experimental data discussed in Section 2

Turbulence at the inlet was specified in terms of turbulence length scale l and turbulence intensity I which are specified as:

$$I = \frac{\sqrt{\frac{2k}{3}}}{V_L} = 10\% \text{ and } l_t = 0.07d \quad (22)$$

A sensitivity analysis revealed that the simulation results are not significantly affected by the numerical values of I and l_t . For each of the inlet velocities investigated the kinetic constant for the LDF model K_M was varied over a range that covers the majority of organic vapours[10] (a range from 0.001 s^{-1} to 0.01 s^{-1})

Validation

The computational method was validated by comparing the breakthrough times for simulations at three different inlet flow rates to the experimental data gathered by the method seen in Section 2. A threshold value of 10ppm cyclohexane at the outlet was considered to be the criteria for breakthrough, as this is this the value used in NIOSH certifications of canister performance[34].

The simulation results for 15 mm beds are listed in Table 1. It is clear from Table 1 that the computational method used here provides a good representation of the breakthrough process.

CFD Results

Analysis of the adsorption performance has been carried out with respect to the distance through the bed that contamination could be seen. The breakthrough front distance was defined as the furthest point in the bed at which the threshold concentration ($1x10^{-6}$ by mass fraction) was present in the vapor phase. The results have been found to be insensitive to the specific choice of threshold. The variation of the front distance L_f over time is shown in Fig. 3 for cases with $K_M = 0.004$ s^{-1} and $K_M = 0.01$ s^{-1}.

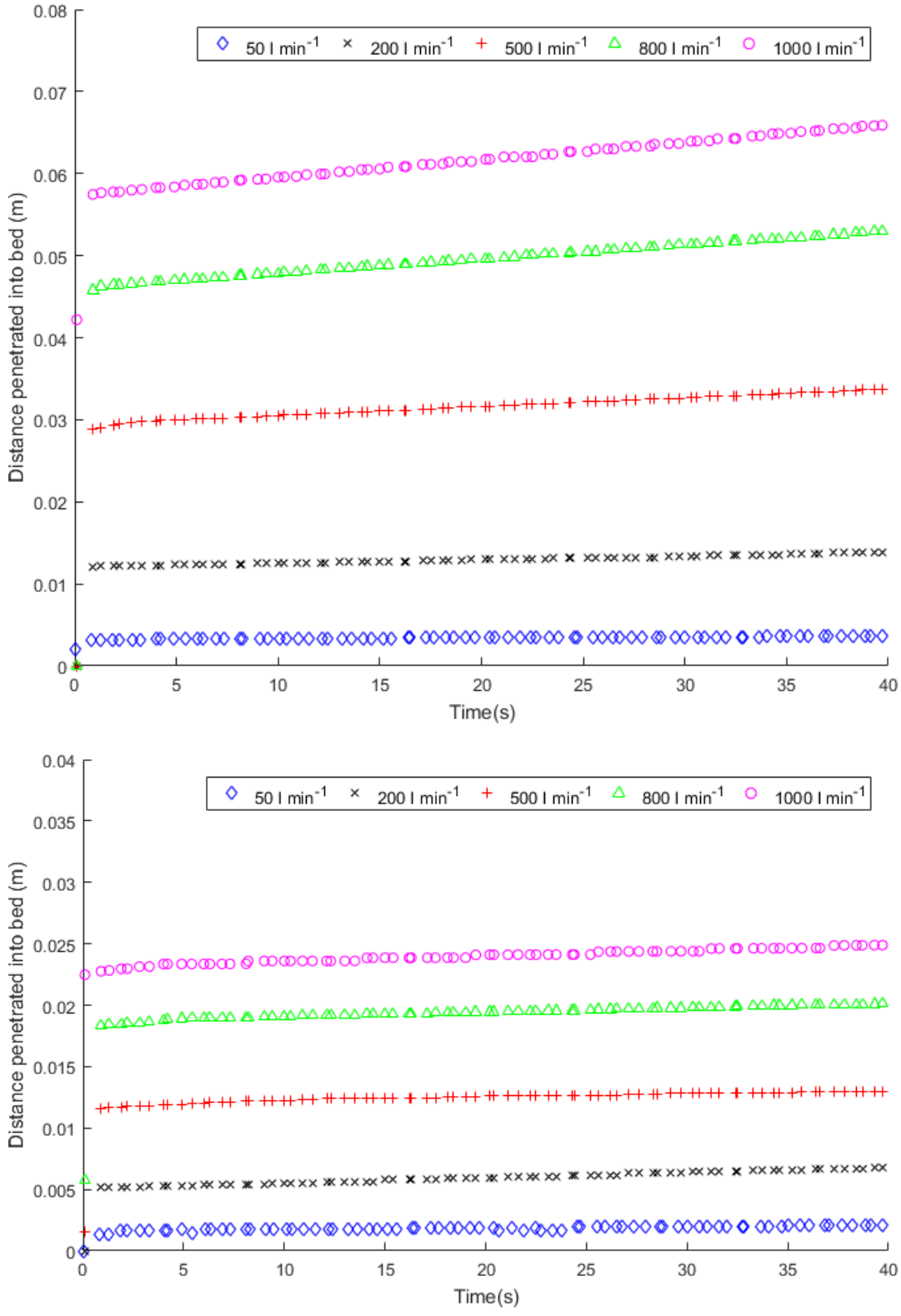

Figure 3: The distance into the bed a threshold vapor concentration of $Y_{C_6H_{12}} = 0.0001$ can be seen for (a) $K_M = 0.004\ s^{-1}$, (b) $K_M = 0.01\ s^{-1}$.

It can be seen from Fig. 3 that a near instant jump in L_f occurs as the contaminant first enters the bed. The magnitude of this initial penetration into the bed is much greater at low values of K_M. In all cases, after this initial penetration into the bed, the front progresses gradually at a reduced speed, v_f, which increases with increased inlet velocity, until breakthrough occurs.

A comparison can be made to the Wheeler-Jonas equation (Eq. 3), which may be re-written to express the front distance (L_f) into the bed over time.

$$L_f = \left(\frac{C_{in}v_{in}}{\rho_B W_e}\right) t + \frac{V_L}{k_{WJ}} \ln\left(\frac{C_{in}}{C_{out}}\right) \quad (23)$$

In this equation, the penetration of the target vapor concentration into the bed is composed of two distinct elements:

- A steady constant increase in penetration length over time, which is independent of the adsorption kinetics.
- An initial, instantaneous penetration into the bed, which is inversely proportional to the kinetic constant.

The relationship between the simulated results and the Wheeler-Jonas model is investigated by separating the bed penetration into two components, the initial penetration length L_{IP} and the front speed v_f. Both these quantities can be defined with respect to some threshold concentration C_{out}.

In the simulated results, L_{IP} can be clearly identified from Fig. 3 as the near instantaneous jump in L_f within the first few seconds of each case, whereas v_f can be identified by the gradient of each set of data in the time that follows the almost instantaneous jump.

The time-independent term of the Wheeler-Jonas equation suggests that the initial breakthrough distance should be inversely proportional to the kinetic constant[35]. The relationship between V_L/K_M and L_{IP} can be seen from Fig. 4 for all cases investigated. It is evident from Fig. 4 that

using the LDF model for adsorption kinetics gives a similar trend to the Wheeler-Jonas model. This behavior appears consistently over the full range of flow rates used in this study.

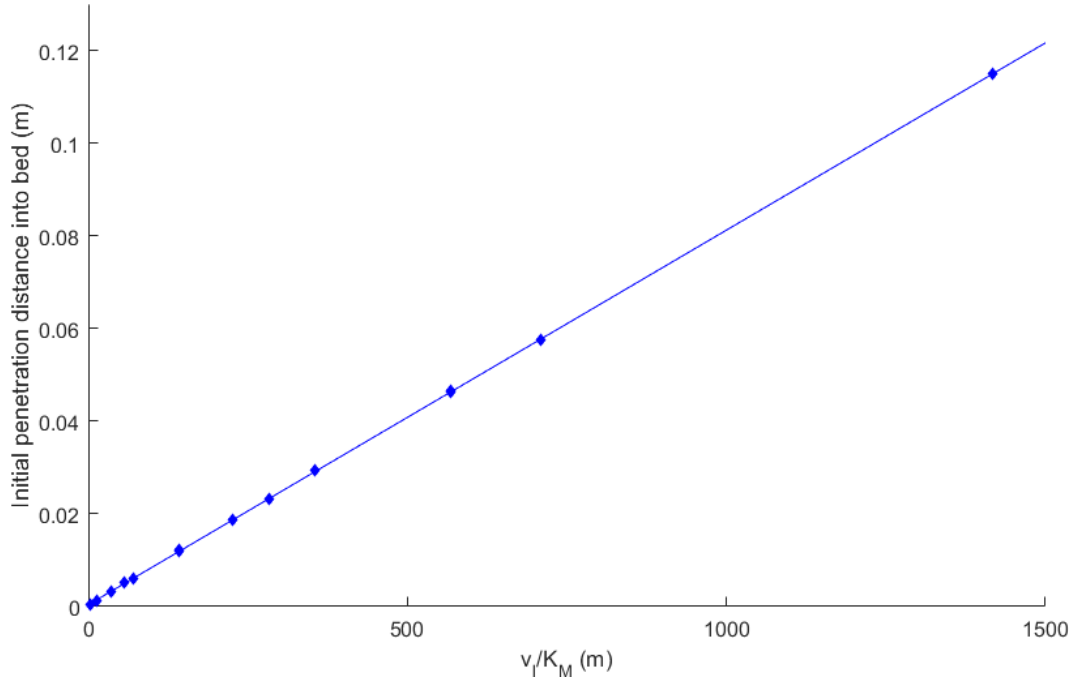

Figure 4: Distance contaminant penetrates into the bed in the initial rapid stage, seen against V_l/K_M

The speed of the front v_{WJ} moving through the bed after the initial period of rapid penetration can be investigated by comparison with that predicted by the Wheeler-Jonas equation as:

$$v_{WJ} = \frac{c_{in}V_L}{\rho_B W_e} \tag{24}$$

where $c_{in}V_L$ gives the rate at which contaminant enters the bed, whereas $\rho_B W_e$ represents the total adsorbent capacity of the bed at equilibrium with the inlet contaminant concentration. This gives v_{WJ} as the rate at which contaminant enters the bed over the adsorption capacity of the bed. The ratio of the front speed seen in the results of the CFD simulations to v_{WJ} is a key parameter for identifying deviations from plug flow in a small activated carbon bed, which is presented in Fig. 5.

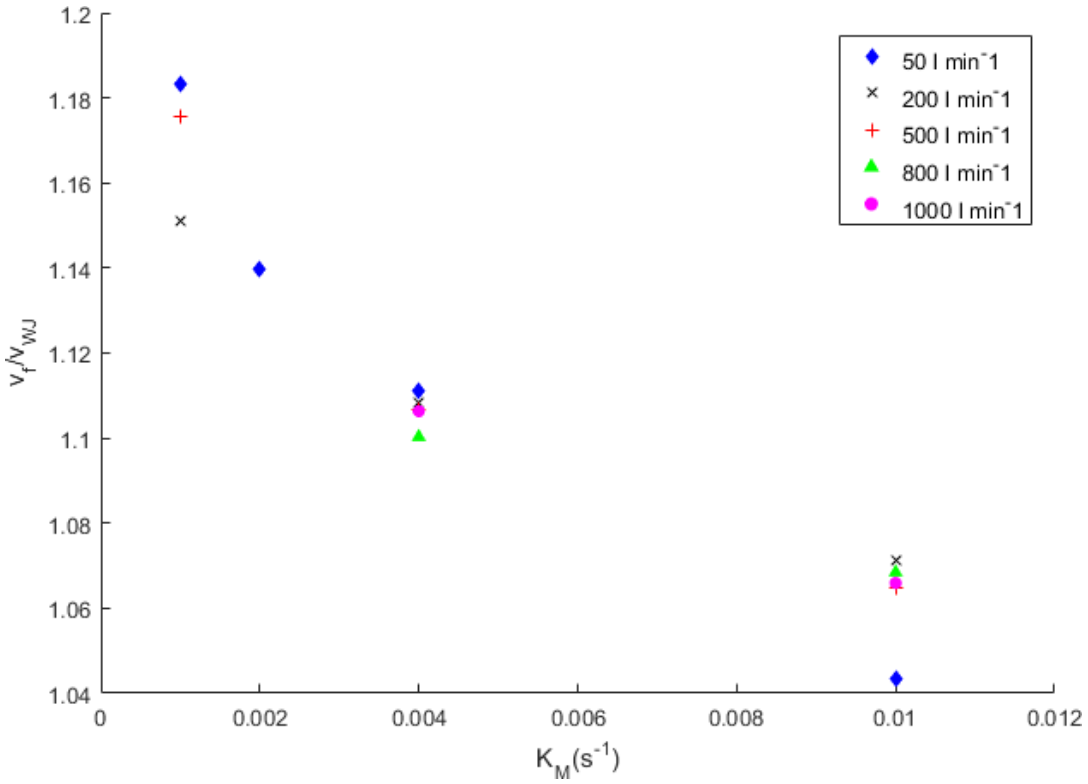

Figure 5: Ratio of front speed to front speed predicted from the Wheeler-Jonas equation for different inlet velocities and values of K_M

As expected, in all cases the front speed slightly exceeds the value that would be predicted by the Wheeler-Jonas equation, as true plug flow is impossible due to the no slip condition at the canister wall. It can be seen from Fig. 5 that there is a slight but significant tendency for lower values of K_M to produce greater front speeds, an effect that is not predicted by the Wheeler-Jonas equation.

An explanation for this kinetic-dependent deviation from the plug flow case may be seen by investigation of the distribution of uptake throughout the bed, as seen for each value of K_M investigated for two example flow rates in Fig. 6.

(a)

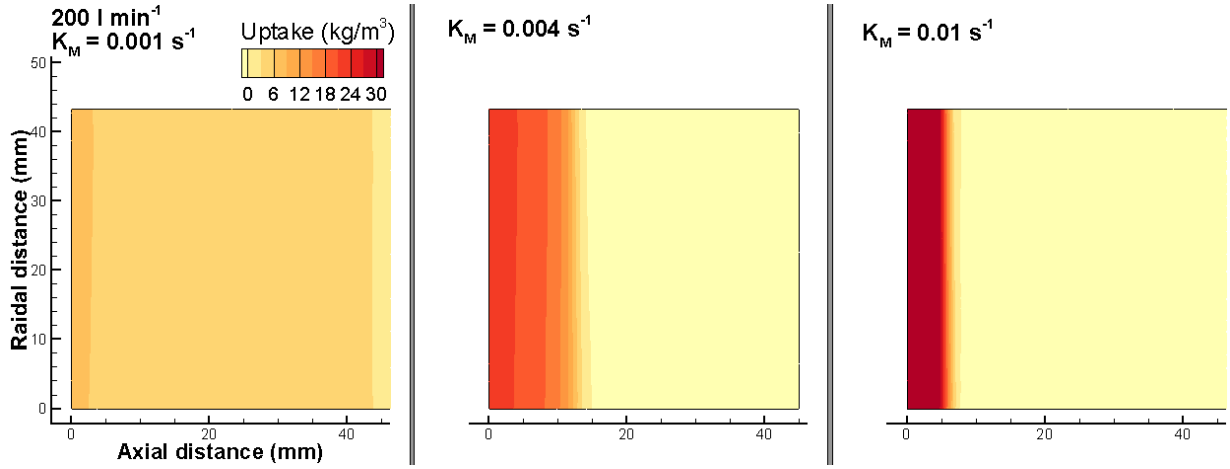

(b)

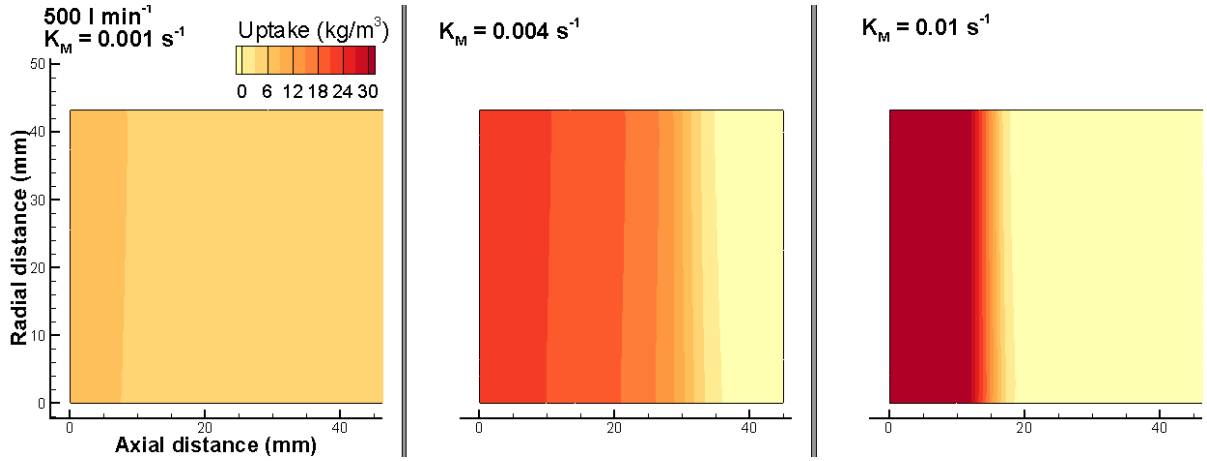

Figure 6: Distribution of uptake of contaminant throughout the bed after 60 s exposure at (a) 200 l min^{-1} (inlet velocity 0.567 m/s) and (b) 500 l min^{-1} (inlet velocity 1.418 m/s).

For each of the cases, after an equivalent time under exposure (and hence an equivalent total amount of contaminant within the bed) the distribution of contaminant can be seen to differ greatly. In general, this results in a greater contaminated volume with slower adsorption kinetics, as the contaminant spreads deeper into the bed. In contrast, when the kinetics are fast a small region of high concentration can be seen.

As adsorption occurs, the volume of fluid flowing through the filter decreases. This will result in a slight reduction in fluid velocity as the flow area remains unchanged. This coupling between the adsorption kinetics and the front speed is not accounted for by the Wheeler-Jonas model. An example of the variation in fluid velocity distributions seen at equivalent flow time is shown in Fig. 7. This is in contrast with a typical uniform bed without adsorption, in which the expected velocity profile is a thin boundary layer at the wall, with plug flow seen throughout the center of the domain [19].

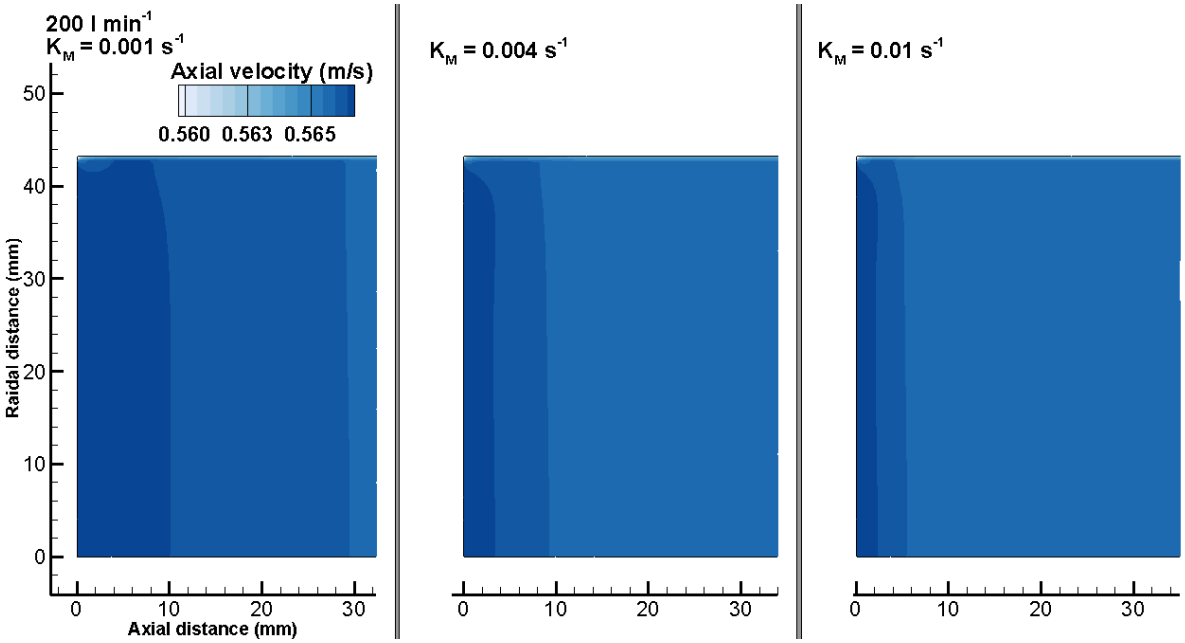

Figure 7: Axial velocity distribution close to the inlet of the bed for an inlet flowrate of 200 l min^{-1} (corresponding to an inlet velocity of 0.567 m/s) seen 60 s after first exposure.

Moreover, the generation of turbulence within the carbon bed may also influence the velocity profile. The generation of turbulent kinetic energy is driven by the velocity gradient, as can be seen from Eq. 14. An increased velocity gradient due to adsorption taking place over a smaller volume (as seen in the cases with faster adsorption kinetics) will result in greater generation of turbulent kinetic energy and alter the velocity profile.

The distribution of contaminant in the inlet stream will also have some impact on the distribution of uptake in the bed, which may affect the speed at which the front then advances through the bed. A sample mass fraction profile just before the contaminant reaches the carbon bed is shown in Fig. 8. Although the contaminant is introduced as a plug flow, a non-uniform radial distribution forms as it flows through the cylinder towards the bed. This is due to the velocity profile caused by the no-slip condition at the wall, and the turbulent mixing in the axial direction towards the axis. This results in a low concentration of contaminant at the centerline reaching the carbon first, and a maximum concentration further from the axis.

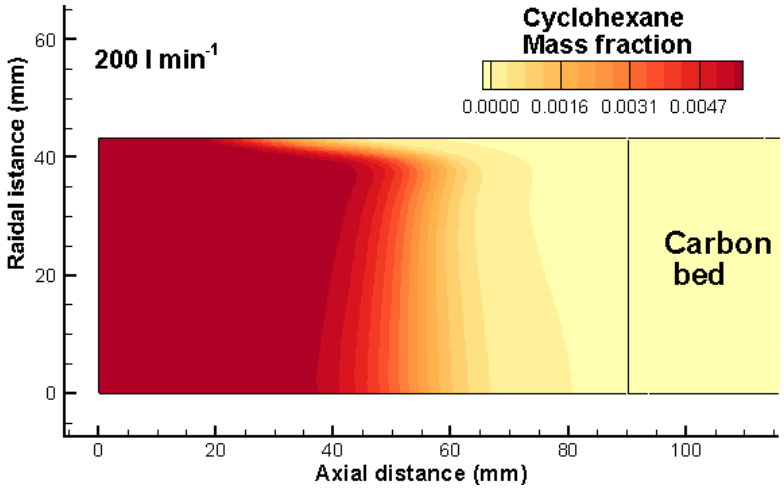

Figure 8: The distribution of contaminant in the inlet stream at 200 l min^{-1} (inlet velocity 0.567 m/s) immediately before it first contacts the carbon bed.

The effect of this distribution can clearly be seen on the shape of the front when the contaminant first penetrates into the bed. Examples of this behavior are shown in Fig. 9 for two different flow rates. Although the first point of entry into the bed occurs along the center line, the axial distribution of contaminant results in a much shorter initial penetration into the bed. In contrast to this, further from the axis where the peak concentration is higher, the initial penetration distance is significantly increased.

(a)

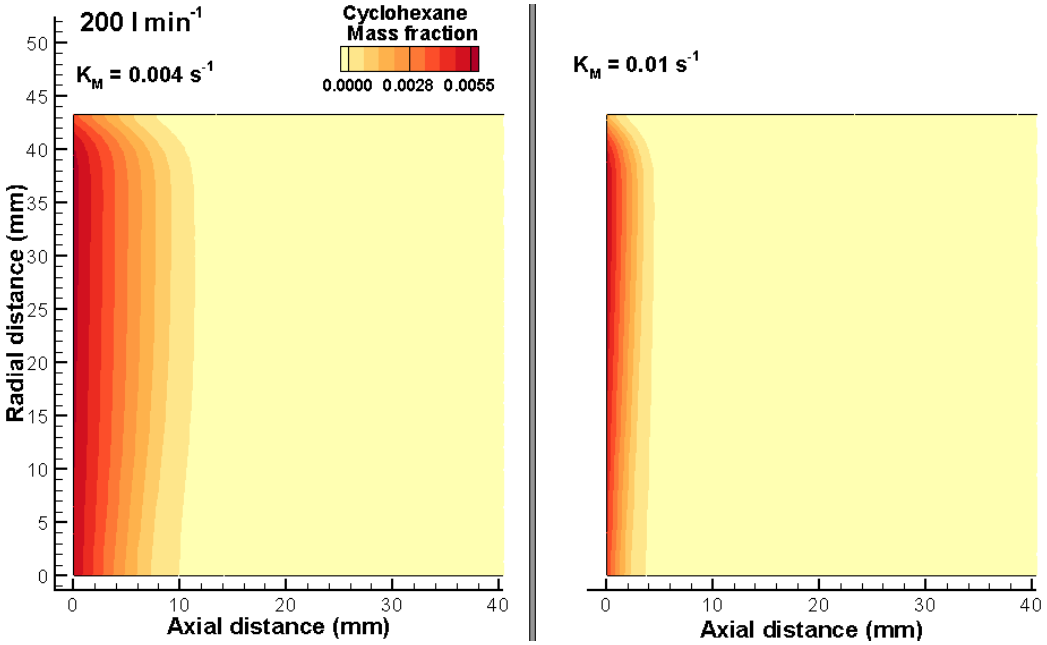

(b)

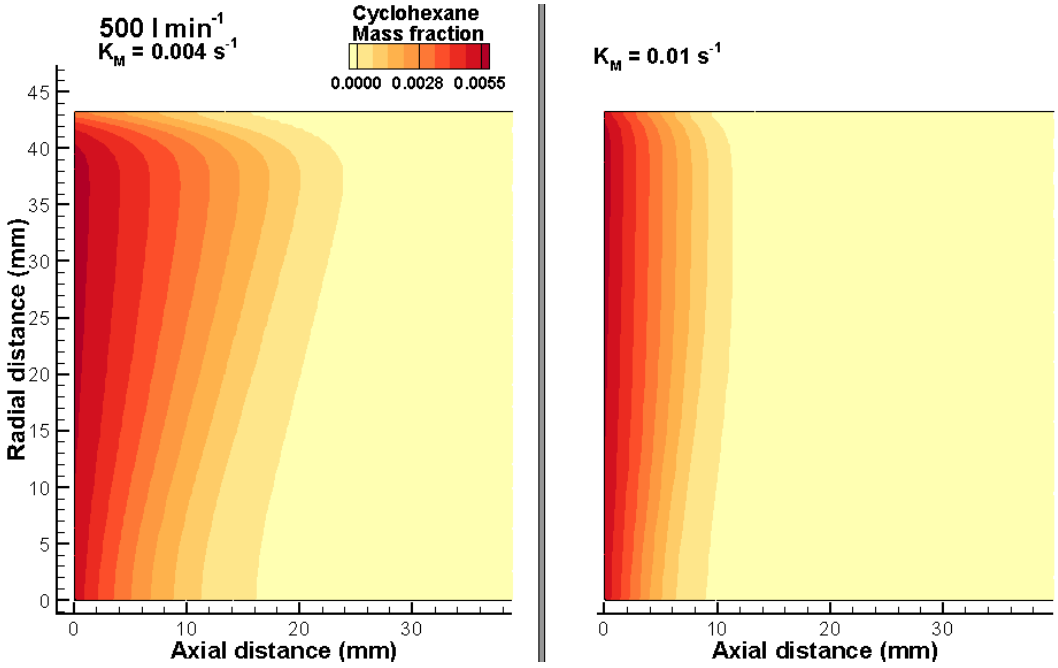

Figure 9: Distribution of contaminant in the carbon bed 0.1 s after initial exposure at (a) 200 l min^{-1} (inlet velocity 0.567 m/s) and (b) 500 l min^{-1} (inlet velocity 1.418 m/s) for $K_M = 0.004\ s^{-1}$ and $K_M = 0.01\ s^{-1}$.

The impact this has later after the initial moment of exposure can be seen in Fig. 10 for flow rates of 200 l min^{-1} and 500 l min^{-1}. A close inspection of the contaminant distribution in the vapor phase close to the center line shows that the adsorption profile in the radial direction at the front is dependent on the adsorption kinetics. At $K_M = 0.004\ s^{-1}$, the maximum distance the threshold cyclohexane concentration is obtained along the axis within the carbon bed. However, for $K_M = 0.01\ s^{-1}$, this maximum distance is found to be slightly offset from the axis, in a manner reminiscent of the profile seen when the contaminant first enters the bed. This suggests that for faster kinetics, the distribution of concentration at the earliest stage of exposure results in an effect, which is retained for much longer. The difference in contaminant distribution at different stages in filter lifetime for different adsorption kinetics may account for the variations in front speed. The precise effect seen here is specific to the geometry considered and the inlet contaminant distribution; however in any case where contaminant is introduced there is likely to be a non-uniform distribution in the inlet stream and a similar relationship between kinetics and entry contaminant distribution.

(a)

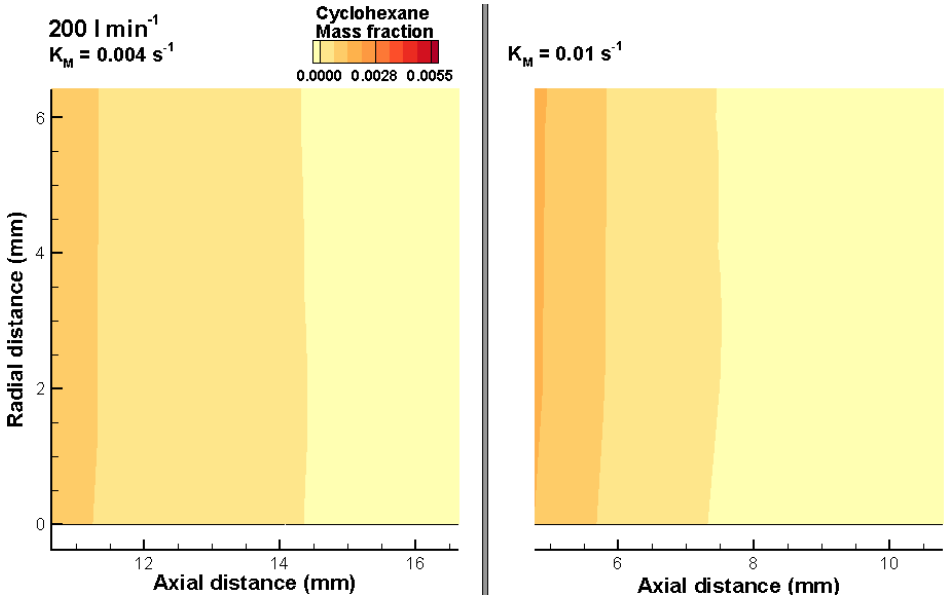

(b)

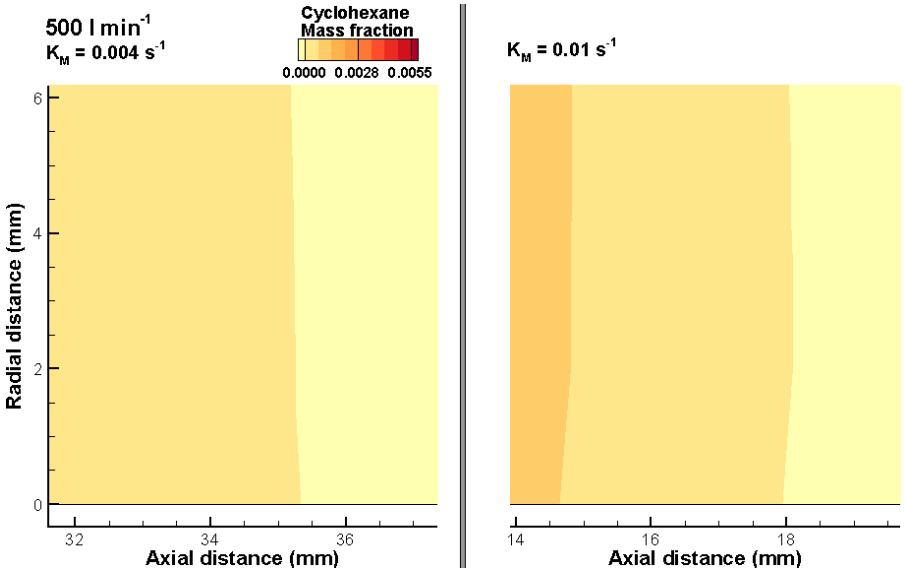

Figure 10: distribution of contaminant close to the center line 60 s after initial exposure at (a) 200 l min^{-1} (0.567 m/s inlet velocity) and (b) 500 l min^{-1} (1.418 m/s inlet velocity) for $K_M = 0.004\ s^{-1}$ and $K_M = 0.01\ s^{-1}$

Conclusions

A numerical model has been developed to predict the flow behavior in small activated carbon adsorbent beds. Cyclohexane has been chosen as the test contaminant and its adsorption was modelled in accordance with the Dubinin-Radushkevich isotherm with linear driving force (LDF) kinetics. Breakthrough times predicted by the model have been shown to provide an excellent match to experimental breakthrough data for cyclohexane. The model has been utilized to analyze the effects of flow rate on adsorption performance so that the assumption of plug flow, which is commonly held as an assumption in the analysis of carbon beds, can be assessed.

Simulations have been carried out over a range of flow rates from 50 l min^{-1} to 1000 l min^{-1}, as it was expected that the deviation from the plug flow assumption would be greater at higher inlet flowrates. The contaminant used represented cyclohexane, to match the experimental data. The LDF kinetic constant has been varied over a range from 0.001 s^{-1} to 0.01 s^{-1}, which is representative of a wide range of volatile organic compounds, to isolate the effects of kinetics on adsorption performance.

The distance at which a threshold contaminant concentration could be seen into the bed at a given time has been investigated over the bed lifetime. In general, it has been noted that a period of very rapid (<1 second) penetration into the bed occurred after the initial exposure. The contaminant (in the vapor phase) has been seen to advance at a constant rate for the rest of the bed lifetime. This behavior is similar to that predicted from the mass-balance derived Wheeler-Jonas equation for plug flow in carbon beds.

It has been found that the initial period of rapid penetration into the bed was directly proportional to the flow velocity and inversely proportional to the kinetic constant ($\propto V_L/K_M$), a trend that was

closely followed for all flow rates and kinetic constants. This was in line with the expected behaviour seen from the plug flow analysis.

The speed at which a front of a given concentration would advance through the bed after this initial period would be expected to be entirely independent of K_M from the plug flow analysis. In all cases, the front speed has been found to be slightly quicker than the plug flow analysis would predict, although over the range of inlet velocities used in this study there was no apparent greater deviation from plug flow for the higher inlet velocities. However, a trend has been seen in which the ratio of front speed seen to the expected plug flow front speed has been found to be greater when the adsorption kinetics were slower.

It can be seen that the kinetics modify the velocity profile throughout the bed, as the volume flow rate of the fluid decreases with adsorption, resulting in an overall decreased velocity downstream. In the cases with fast kinetics, the adsorption takes place over a smaller overall volume of carbon, resulting in a more rapid fluid deceleration. This increased velocity gradient in the axial direction will result in increased generation of turbulence, which may modify the flow field.

Additionally, the concentration profile of contaminant in the inlet stream at the moment of first exposure affects the shape of the contaminated region in the bed. The contaminant has been found to enter the carbon bed first at the axis but at a lower concentration, while the peak concentration at the earliest stages of exposure will be seen further from the axis. This results in the contaminated front in the early stages of exposure having a distinctive shape where the furthest contaminated distance into the bed does not fall on the center line. In the cases with low kinetic constants, this front shape has been obtained only shortly after initial exposure. However, in the cases with fast kinetics the forward-most contaminated point in the bed has been found to be offset from the axis

for the whole duration of the simulation. This suggests that there is a “history” effect of the inlet contaminant distribution when the adsorption kinetics are fast. The precise nature of this effect is likely to vary with different inlet contamination profiles.

Acknowledgements

SW and NC have received funding from the Engineering and Physical Sciences Research Council (EPSRC), UK (Grant number OSR/0590DT15/CASE) and the Defence Science and Technology Laboratory, UK (Grant number RES/0590/7321).

Nomenclature

Symbol	Definition	Units
a_1	Viscous resistance	kg m^{-3} s^{-1}
a_2	Inertial resistance	kg m^{-4}
C_{in}	Inlet concentration	kmol/m^3
C_{out}	Threshold outlet concentration	kmol/m^3
C_μ, C_l^*	Turbulence model parameter	(-)
D_a	Mass diffusion coefficient of species a	m^2 s^{-1}
d_p	Particle diameter	m
E_0	Adsorption energy	J/kmol
J_a	Flux of species a	kg m^{-2} s^{-1}
k_{eff}	Effective thermal conductivity	W m^{-1} K^{-1}
K_M	Effective mass transfer kinetic constant	s^{-1}
l_ϵ, l_μ	Turbulence model length scales	(-)
M_W	Molecular weight	kg/kmol
Re_y	Turbulent Reynolds number	(-)
$\bar{S}_{\alpha,i}$	Species source term	kg m^{-3} s^{-1}
$\bar{S}_{ei}$	Energy source term	J m^{-3} s^{-1}
$\bar{S}_{ui}$	Momentum source term	kg m^{-2} s^{-2}
Sc_t	Turbulent Schmidt number	(-)
t_b	Breakthrough time	s
v_{WJ}	Wheeler-Jonas front speed	m/s
V_L	Inlet velocity	m/s
W	Uptake	(-)
W_0	Micropore volume	m^3/kg
W_e	Equilibrium uptake	(-)
α	Mass fraction	(-)
β	Affinity coefficient	(-)
ϵ	Turbulent energy dissipation rate	J m^{-3} s^{-1}
λ_ϵ	Turbulence model blending parameter	(-)
μ_l	Dynamic viscosity	m^2/s
μ_t	Turbulent viscosity	m^2/s
σ_k, σ_ϵ	Turbulence model parameters	(-)

References

(1) Oh, K.-J.; Park, D.-W.; Kim, S.-S.; Park, S.-W., Breakthrough Data Analysis of Adsorption of Volatile Organic Compounds on Granular Activated Carbon. *Korean J. Chem. Eng.* **2010,** *27*, 632-638.
(2) Suyadal, Y.; Erol, M.; Oğuz, H., Deactivation Model for the Adsorption of Trichloroethylene Vapor on an Activated Carbon Bed. *Ind. Eng. Chem. Res.* **2000,** *39*, 724-730.
(3) Park, S. W.; Choi, B. S.; Lee, J. W., Breakthrough Data Analysis of Adsorption of Toluene Vapor in a Fixed-Bed of Granular Activated Carbon. *Sep. Sci. Technol.* **2007,** *42*, 2221-2233.
(4) Dubinin, M., The Potential Theory of Adsorption of Gases and Vapors for Adsorbents with Energetically Nonuniform Surfaces. *Chem. Rev.* **1960,** *60*, 235-241.
(5) Chen, S. G.; Yang, R. T., Theoretical Basis for the Potential Theory Adsorption Isotherms. The Dubinin-Radushkevich and Dubinin-Astakhov Equations. *Langmuir* **1994,** *10*, 4244-4249.
(6) Dubinin, M. M., *Progress in Surface and Membrane Science*. Academic Press, New York: 1975; Vol. 9.
(7) Nguyen, C.; Do, D. D., The Dubinin–Radushkevich Equation and the Underlying Microscopic Adsorption Description. *Carbon* **2001,** *39*, 1327-1336.
(8) Lodewyckx, P.; Wood, G. O.; Ryu, S. K., The Wheeler–Jonas Equation: A Versatile Tool for the Prediction of Carbon Bed Breakthrough Times. *Carbon* **2004,** *42*, 1351-1355.
(9) Wood, G. O., Affinity Coefficients of the Polanyi/Dubinin Adsorption Isotherm Equations: A Review with Compilations and Correlations. *Carbon* **2001,** *39*, 343-356.
(10) Reid, C. R.; Thomas, K. M., Adsorption Kinetics and Size Exclusion Properties of Probe Molecules for the Selective Porosity in a Carbon Molecular Sieve Used for Air Separation. *The Journal of Physical Chemistry B* **2001,** *105*, 10619-10629.
(11) Fletcher, A. J.; Yuzak, Y.; Thomas, M., Adsorption and Desorption Kinetics for Hydrophilic and Hydrophobic Vapors on Activated Carbon. *Carbon* **2006,** *44*, 989-1004.
(12) Wheeler, A.; Robell, A. J., Performance of Fixed-Bed Catalytic Reactors with Poison in the Feed. *J. Catal.* **1969,** *13*, 299-305.
(13) Jonas, L. A.; Rehrmann, J. A., The Kinetics of Adsorption of Organo-Phosphorus Vapors from Air Mixtures by Activated Carbons. *Carbon* **1972,** *10*, 657-663.
(14) Jonas, L. A.; Rehrmann, J. A., Predictive Equations in Gas Adsorption Kinetics. *Carbon* **1973,** *11*, 59-64.
(15) Wood, G. O.; Lodewyckx, P., An Extended Equation for Rate Coefficients for Adsorption of Organic Vapors and Gases on Activated Carbons in Air-Purifying Respirator Cartridges. *AIHA J.* **2003,** *64*, 646-650.
(16) Papurello, D.; Tomasi, L.; Silvestri, S.; Santarelli, M., Evaluation of the Wheeler-Jonas Parameters for Biogas Trace Compounds Removal with Activated Carbons. *Fuel Process. Technol.* **2016,** *152*, 93-101.
(17) Haghighat, F.; Lee, C.-S.; Pant, B.; Bolourani, G.; Lakdawala, N.; Bastani, A., Evaluation of Various Activated Carbons for Air Cleaning – Towards Design of Immune and Sustainable Buildings. *Atmos. Environ.* **2008,** *42*, 8176-8184.
(18) Wu, J.; Claesson, O.; Fangmark, I.; Hammarstrom, L.-G., A Systematic Investigation of the Overall Rate Coefficient in the Wheeler–Jonas Equation for Adsorption on Dry Activated Carbons. *Carbon* **2005,** *43*, 481-490.

(19) Chandrasekhara, B. C.; Vortmeyer, D., Flow Model for Velocity Distribution in Fixed Porous Beds under Isothermal Conditionsmodell Der Geschwindigkeitsverteilung in Einem Isotherm Durchströmten Festbett. *Wärme-und Stoffübertrag.* **1979,** *12*, 105-111.
(20) Li, C., Aerodynamic Behaviour of a Gas Mask Canister Containing Two Porous Media. *Chem. Eng. Sci.* **2008**, 1832-1843.
(21) Su, Y.-C.; Li, C.-C., Computational Fluid Dynamics Simulations and Tests for Improving Industrial-Grade Gas Mask Canisters. *Adv. Mech. Eng.* **2015,** *7*, 1687814015596297.
(22) Taylor, K.; Smith, A.; Ross, S.; Smith, M., Cfd Modelling of Pressure Drop and Flow Distribution in Packed Bed Filters. *PHOENICS J. Comput. Fluid. Dyn. Appl.* **2000,** *13*, 399-413.
(23) NIOSH, Statement of Standard for Chemical, Biological, Radiological and Nuclear (CBRN) Full Facepiece Air Purfying Respirator. NIOSH: Washington, DC, 2003.
(24) Wang, G.; Dou, B.; Zhang, Z.; Wang, J.; Liu, H.; Hao, Z., Adsorption of Benzene, Cyclohexane and Hexane on Ordered Mesoporous Carbon. *J. Environ. Sci.* **2015,** *30*, 65-73.
(25) Harris, E. Improvements in or Relating to the Filling of Granular Materials into Containers. UK Patent 606,867, 1946.
(26) ANSYS, *Academic Research, Release 16.2*. Ansys: 2016.
(27) Patankar, S., *Numerical Heat Transfer and Fluid Flow*. Hemisphere Publishing Corportation: 1980.
(28) Wood, S. G. A.; Chakraborty, N.; Smith, M. W.; Summers, M. J., A Computational Fluid Dynamics Analysis of Transient Flow through a Generic Chemical Biological Radiological and Nuclear Respirator Canister. *Chem. Eng. Res. Des.* **2019,** *142*, 13-24.
(29) Heeb, T. G.; Brodkey, R. S., Turbulent Mixing with Multiple Second-Order Chemical Reactions. *AlChE J.* **1990,** *36*, 1457-1470.
(30) Das, A. K.; De Wilde, J.; Heynderickx, G. J.; Marin, G. B., CFD Simulation of Dilute Phase Gas–Solid Riser Reactors: Part Ii—Simultaneous Adsorption of SO2–NOx from Flue Gases. *Chem. Eng. Sci.* **2004,** *59*, 187-200.
(31) Wood, S. G. A.; Chakraborty, N.; Smith, M. W.; Summers, M. J.; Brewer, S. A., The Impact of Canister Geometry on Chemical Biological Radiological and Nuclear Filter Performance: A Computational Fluid Dynamics Analysis. *J. Occup. Environ. Hyg.* **2018**, 1-35.
(32) Suzin, Y.; Nir, I.; Kaplan, D., The Effect of Flow Pattern on Adsorption of Dimethyl Methyl Phosphonate in Activated Carbon Beds and Canisters. *Carbon* **2000,** *38*, 1129-1133.
(33) Berezhnoi, A. N.; Semenov, A. V., *Binary Diffusion Coefficients of Liquid Vapors in Gases*. Begell House New York: 1997.
(34) NIOSH, Determination of CBRN Organic Vapor (Cyclohexane) Service Life Test, Air Purifying Respirators Standard Test Procedure (Stp) CET-APRS-STP-CBRN-0301. Centers for Disease Control and Prevention: https://www.cdc.gov/niosh/npptl/stps/aprespcbrn.html, 2005.
(35) Grévillot, G.; Marsteau, S.; Vallières, C., A Comparison of the Wheeler-Jonas Model and the Linear Driving Force at Constant-Pattern Model for the Prediction of the Service Time of Activated Carbon Cartridges. *J. Occup. Environ. Hyg.* **2011,** *8*, 279-288.

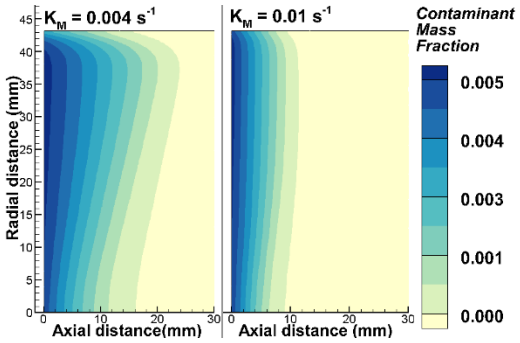

For table of contents only